ASSESSMENT OF STATISTICAL SAMPLING METHODS AND APPROXIMATION MODELS APPLIED TO AEROACOUSTIC AND VIBROACOUSTIC PROBLEMS

Till M. Biedermann[1*], Marius Reich[2], F. Kameier[1], M. Adam[2], C.O. Paschereit[3]

[1]Institute of Sound and Vibration Engineering ISAVE
University of Applied Sciences Duesseldorf, Duesseldorf 40476, Germany
[*]Email: till.biedermann@hs-duesseldorf.de

[2]Centre of Innovative Energy Systems ZIES
University of Applied Sciences Duesseldorf, Duesseldorf 40476, Germany

[3]Institute of Fluid Dynamics and Technical Acoustics
Technical University Berlin, Berlin 10623, Germany

ABSTRACT

The effect of multiple process parameters on a set of continuous response variables is, especially in experimental designs, difficult and intricate to determine. Due to the complexity in aeroacoustic and vibroacoustic studies, the often-performed simple one-factor-at-a-time method (OFAT) turns out to be the least effective approach. In contrast, the statistical design of experiments (DOE) is a technique used with the objective to maximize the obtained information while keeping the experimental effort at a minimum. With the obtained information being objective and valid, a parametric or non-parametric approximation of each response variable can be performed, leading to an enhanced understanding of the underlying physical principles as well as to a fast and efficient analysis in the form of graphical representation, (multi-objective) optimisation or basic prediction. The presented work aims at giving insights on DOE applied to aeroacoustic and vibroacoustic problems while comparing different experimental designs and approximation models. For this purpose, an experimental rig was developed where a ducted low-speed fan is installed. The rig allows to gather data of both, aerodynamic and aeroacoustic nature. Altogether, three independent process parameters are analysed, namely the incoming turbulence intensity, the rotational speed and the throttling state. The experimental designs used to sample the design space are a circumscribed central

composite design (C-CCD) and a Box-Behnken design (BBD), both used to model a response surface regression, and Latin Hypercube sampling (LHS) to model an Artificial Neural Network (ANN). The dependent response variables are the overall sound pressure level as well as the aerodynamic performance and the vibrational signal at the fan hub. The approximation models are rated by means of the number of necessary experiments and the resulting accuracy on evenly distributed test data. The results indicate that, even though more experiments are required, LHS extracts information that is more diverse and, in combination with a light ANN, outperforms the quadratic response surface regressions using the information collected by both, the CCD as well as the BBD. Due to the non-collapsing attribute of the Latin Hypercube sampling, further experiments can easily be added and thus increasing the accuracy. It can be shown that the LHS, initially developed for computer-aided experiments, can also be used as an experimental design.

1   INTRODUCTION

The acoustic signature of axial fans and blowers is known to be highly affected by the specific inflow conditions [1–3]. At smooth inflow conditions the acoustic signature of a fan is mainly limited to noise radiation from the rotor trailing edges, struts as well as rotor speed-dependent effects like e.g. the blade passing frequency and rotor stator interaction. At given inflow conditions of elevated turbulence intensities, however, a significant portion of leading edge noise of broadband character is added, which is able to dominate the acoustic signature of a fan in the low-to-intermediate frequency region, plus the occurrence of possible additional effects within the rotor like e.g. the altering of flow separation phenomena etc. Recent research focussed on the establishment and evaluation of passive noise reduction mechanisms in order to significantly reduce the turbulence-induced leading edge noise [4, 5].

As it is a commonly reported problem in aeroacoustic optimisation, opposing trends arise for the targets of low-noise-design while keeping the aerodynamic efficiency on high levels. Motivated by the described problematic the question arose on how to describe a multi-parameter system best by taking into account target values of aerodynamic and aeroacoustic nature. Common statistical-empirical modelling approaches such as the Design of Experiments (DoE) methodology [6, 7] are limited to models of second order, and were suspected not to be sufficient to describe systems of high complexity at the desired high prediction accuracy, as it is also concluded by this paper. Thus, these modelling approaches are compared to more advanced Artificial Neural Networks which are unlimited in terms of functional complexity using a Latin Hypercube design, initially designed for numerical simulations [8]. These approaches were used to model both, the aerodynamic and aeroacoustic performance of an axial fan by varying three continuous parameters, namely the fan speed, the throttling state as well as the level of incoming turbulence. The novelty is such that experimental designs are usually adopted for numerical approaches [9] but now a promising modelling approach from the numeric environment is back transferred and applied to an experimental test rig.

2   STATISTICAL APPROACH

To sample the design space in a way that maximum information can be obtained while keeping the number of experimental runs at a minimum, so-called experimental designs, which have to be defined prior the experimental study, are often used. For this study, three different experimental designs are used and compared by means of number of necessary experiments and the resulting accuracy on evenly distributed test data. The first experimental design is the Circumscribed Central Composite design (C-CCD). The C-CCD consists of a two-level factorial design, so called *star points* that lie at the borders of the design space as well as numerous centre points to establish predefined statistical properties, which are for this case

orthogonality and rotatability. Consequently, the C-CCD has five levels for each factor as can be seen in Figure 1 (top right).

The second experimental design is the Box Behnken Design (BBD), which is a fractional three level design, exhibiting orthogonal statistical properties. Contrary to the factorial core of the C-CCD, where the factor levels are located at the corners of the experimental space, the BBD uses factor combinations at the middle of the edges of the design space. Both, the C-CCD and the BBD, are used to model a quadratic response surface regression.

In contrast to the latter designs, the Latin Hypercube sampling was initially developed for computer-aided experiments and thus requires as much levels as the number of runs. To gather as much information as possible, every factor combination is unique. The creation of a LHS is stochastic, which is the reason why designs of more advantageous or disadvantageous nature can be created. To assess different designs, one or more criteria need to be used. For this case study, a metric and a correlation criteria have been used to rate 15.000 different designs. For additional information, a fractional two-level design has been added. The so created LHS can be seen in the bottom left of Figure 1. Due to a lack of orthogonality for quadratic and interaction effects, the LHS is not used for modelling a quadratic response surface regression but for training an Artificial Neural Network (ANN). With this purpose, the LHS is randomly split into training and validation data to train an ANN with a random structure and to monitor this training.

To test the generated models against independent data, ten additional measurements were conducted, where six measurements of this set cover uniform distributed locations within the design space. The remaining four measurements, however, are located at the outer corners of the experimental space which are traditionally hard to approximate by any statistic model. This set of data serves, in addition to the models' coefficient of determination, as quality characteristic for the single chosen approaches.
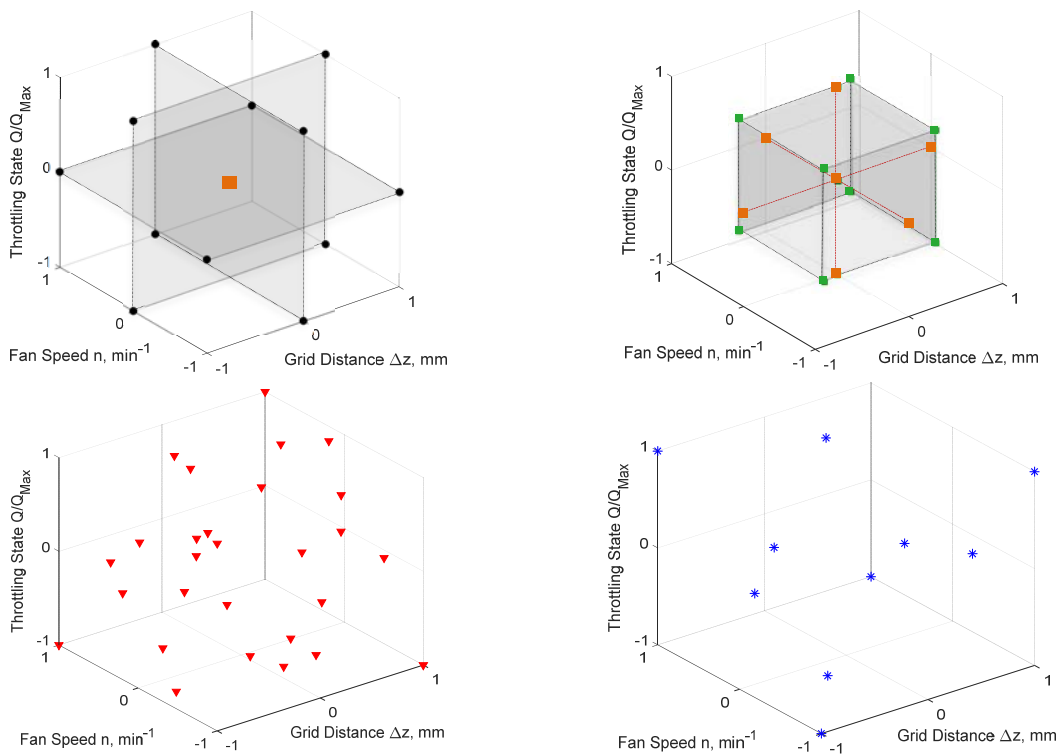

Figure 1: Sampling of experimental space via Box Behnken Design (top left), Central Composite Design (top right) and Latin Hypercube Design (bottom left). Additional test data for validation (bottom right).

3 EXPERIMENTAL SETUP

3.1 Test rig and rotor design

According to DIN ISO 5136 [10] a test rig (Figure 2), enabling the simultaneous measurement of the aerodynamic and aeroacoustic performance, was utilised to analyse a self-designed rotor following the single aerofoil design technique [11]. The rotor consists of six equidistantly distributed blades of C = 0.075 m chord and S = 0.1 m in span where the blades follow the NACA65(12)-10 high-lift aerofoil shape (Figure 3). The fan design is of especially low complexity, thus no sweep, dihedral or shroud of the blades is applied in order to focus on the main aeroacoustic noise sources and avoid possible masking and superimposing effects. The rotor is placed in a duct of D = 0.4 m in diameter, where the mounting takes place via eight struts downstream of the rotor, which itself are vibroacoustically decoupled from the duct to block the occurrence and propagation of solid-borne sound.
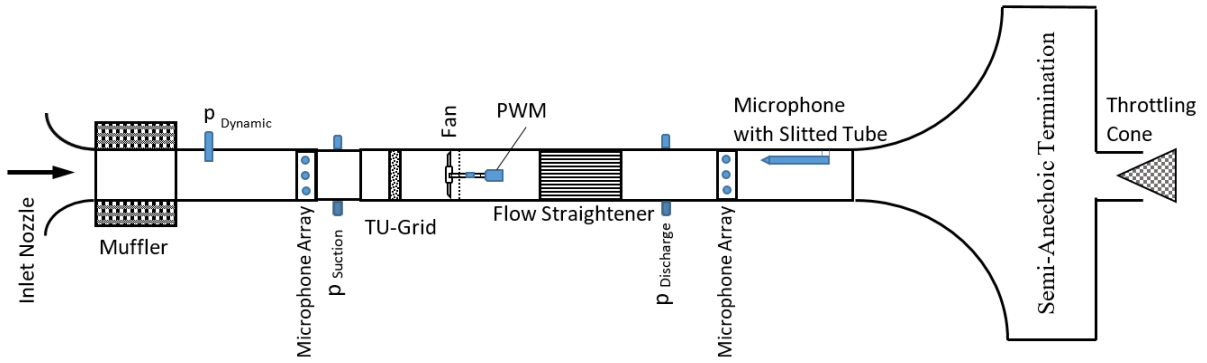

Figure 2: Test rig according to DIN ISO 5136.

3.2 Measurement technique

On the suction and discharge side of the fan the rig was equipped with three ¼-inch condenser microphones each, distributed equidistantly in the circumferential direction (Figure 2). The microphones were used flush-mounted, where a side vented pressure field design allowed for correct equalisation of atmospheric pressure. Additionally, a ½-inch condenser microphone with a slitted tube (turbulence screen) was mounted on the discharge side to gather additional aeroacoustic information. At a sampling rate of 44.1 kHz and a blocksize of 32768 spectral data of up to 17 kHz could be analysed at a frequency resolution of Δf = 1.3 Hz. Applying Hanning windows with an overlap of 66%, the blocks were averaged for 300 times, yielding a total measurement duration of 74 seconds. The rotor speed was monitored via a triaxial acceleration sensor (Δf = 0.25 Hz), mounted on the hub-support. In terms of aerodynamics, a pitot tube, located at the inlet nozzle, was used to measure the flow rate $\dot{Q}$ where the rise of static pressure Δp was obtained via two rings of pressure-tabbing points on the suction and discharge side of the fan, leading to a circumferentially averaged pressure of high accuracy. The power P_{Elec} of the pulse-width-modulated e-motor was obtained by use of a measuring calliper, leading to the systems efficiency η_{System} (Equation 1) of the fan. The aerodynamic data acquisition took place by applying a number of 20 averages.

$$\eta_{System} = \frac{\dot{Q} \cdot \Delta p}{P_{Elec}} \tag{1}$$

Upstream of the fan, a biplane square grid is used to generate elevated turbulent inflow levels, where a ratio of five between grid bar diameter and mesh width proved to result in turbulence levels of good isotropic character [12] at a sufficient distance from the grid. Usually,

analysing different level of turbulence results in the definition of multiple grids with appropriate parameters. In the present case, however, continuously adjustable influencing parameters are desired, thus, the distance between grid and rotor inside the duct was altered what results in an altering of the turbulence levels (see Figure 6).
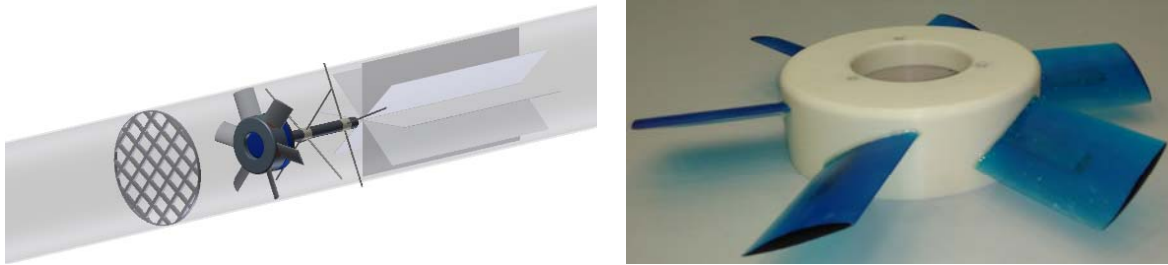

Figure 3: Grid-Fan-Strut assembly within the test rig, including a flow straightener according to DIN ISO 5801(left). Photograph of investigated rotor (right).

3.3 Test matrix and response variables

The chosen experimental space is of three dimensions, defined by the distance between grid and rotor Δz, the throttling state $\delta_{Throttle}$ and the fan speed n_{Rot}. The throttling state δ defines the percentaged and negated flow rate of the system according to Equation 2, independent of the fan speed, where 0% indicates an unrestricted system and vice versa. The variation of these parameters is expected to provide sufficient information on the systems performance that can be described by response variables still to be defined. For the statistical approaches by means of the Design of Experiments methodology the influencing parameters need to be varied on three levels for the Box Behnken Design and on five levels for the Central Composite Design to satisfy the model complexity condition of order two. For the Latin Hypercube sampling, required for the Artificial Neural Network, however, a number of variations in accordance to the amount of model data, is required. Despite the differences in the modelling approaches, the outer limits of each factor are fixed as Table 1 indicates.

$$\delta_{Throttling} = 1 - \frac{\dot{Q}}{\dot{Q}_{Max}} \cdot 100\% \tag{2}$$

Table 1: Limits of experimental space. Absolute values (left) and normalised values (right).

Type	Unit	Min	Max	Type	Unit	Min	Max
Δz_{Grid}	[mm]	100	500	Δz_{Grid}	[--]	-1	+1
$\delta_{Throttle}$	[%]	0	100	$\delta_{Throttle}$	[--]	-1	+1
n_{Rot}	[min^{-1}]	1000	2000	n_{Rot}	[--]	-1	+1

The definition of appropriate response variables turns out to be the crucial part of evaluating a given system as these variables are required to describe the systems characteristic performance with the necessary accuracy. Moreover, they need to be describable by means of the chosen influencing parameters. As has already been mentioned in *Section 1*, the response variables are of aerodynamic and aeroacoustic/ vibroacoustic nature and are listed as follows in Table 2. Aerodynamic parameters are the pressure rise Δp_{Aero} between suction and discharge side of the fan as well as the corresponding flow rate Q_{Aero}. The systems efficiency η_{System} according to Equation 1 defines the third response variable. In terms of acoustics the linear acoustic pressures of the suction side $p_{Suction}$ and the discharge side $p_{Discharge}$, including the acoustic signature of the slitted tube measurements p_{ST} were decided to be implemented in the model as sound pressure levels would distort effects due to the logarithmic scaling. The acoustic pressure of both, the suction and discharge side was obtained by integrating the spectral energies in a

bandpass of 100 Hz $\leq$ f $\leq$ 10 kHz where the lower frequency was chosen due to limitations in the measurement environment. Vibroacoustic effects are incorporated in form of acceleration a_{Hub} on the fan hub-support at frequencies of 0 Hz $\leq$ f $\leq$ 5 kHz.

Table 2: Response variables of the analysed system.

Classification	Aerodyn.	Aerodyn.	Aerodyn.	Acoustics	Acoustics	Acoustics	Vibroacoustics
Type	Pressure	Volume flow	Efficiency	Pressure	Pressure	Pressure	Acceleration
Abbr.	Δp_{Aero}	Q_{Aero}	η_{System}	$p_{Suction}$	$p_{Discharge}$	p_{ST}	a_{Hub}
Unit	[Pa]	[m³s⁻¹]	[%]	[Pa]	[Pa]	[Pa]	[ms⁻²]

4 PRELIMINARY INVESTIGATIONS

For further analysis and accurate modelling of the fan performance, it is essential that aerodynamic similarity laws are valid. With this purpose the dimensional analysis helps to compare the fan performance at various operation conditions and to draw conclusions on the stability of the system within the covered experimental space. The non-dimensional pressure values ψ and flow values φ in Equation 3 – 4, where U is the circumferential velocity and A the through-flow area of the fan, lead to the elimination of the influence of the fan speed, reducing the throttling curves to a single curve as shown in Figure 4 (left). On this basis the percentaged throttling state (Figure 4 – right), independent of the fan speed, can be defined using a function of 6th order, where a coefficient of determination R² = 0.9987 was reached, which is defined as the quotient of the variance of predicted vs. observed values of the data set.

$$\Psi = \frac{\Delta p / \rho}{U^2 / 2} \tag{3}$$
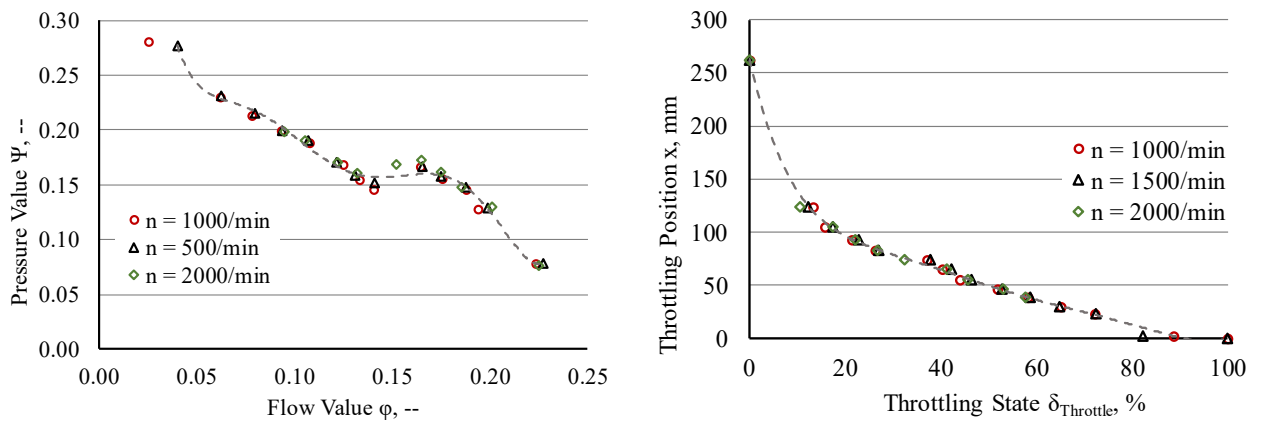
$$\Phi = \frac{Q}{UA} \tag{4}$$

Figure 4: Non-Dimensional fan performance curves (left) and throttling position x as function of throttling state $\delta_{Throttle}$ (right). Dashed lines represent polynomial regression models of 6th order.

4.1 Inflow conditions

To obtain information on both, the local velocity distribution and the distribution of the grid-generated turbulence along the duct radius, 1-D hot wire measurements were conducted by use of a rotating channel, where the hot wire probe can be traversed in the circumferential direction. Figure 5 shows the results with an increment of 10 deg or 53690 averaged samples per step, respectively. Turbulence intensity and velocity are inversely proportional, thus leading to low Tu levels at high mean velocities and vice versa. Overall, the centre region (R = ± 0.1 m) and the outer region (-0.2 m ≤ R ≤ 0.2 m) of the duct show an adequate homogeneity in circumferential direction where the radial trend shows a region of higher velocity (U_0 = 12.5 ms^{-1}) in the centre and reduced velocity (U_0 = 9 ms^{-1}) in the outer region.

Averaging velocity and turbulence intensity over a radius of R = 0.15 m, to avoid the influence of the wall boundary layer, yields a mean velocity of $\overline{U_0}$ = 11.8 ms^{-1} and a turbulence intensity of $\overline{Tu}$ = 7.8 %.
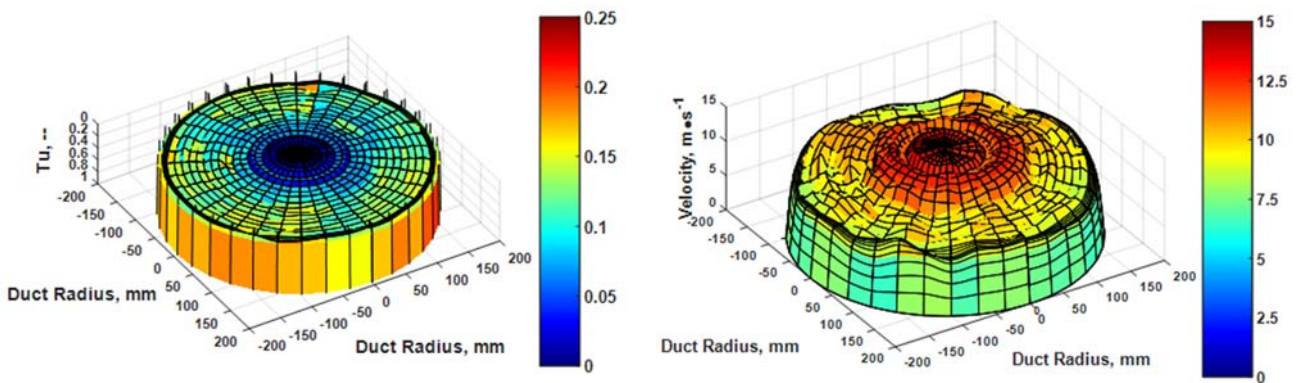

Figure 5: Profiles of turbulence intensity (left) and axial velocity (right) at imaginary position of rotor with turbulence grid at intermediate distance Δz = 300 mm, n = 2400 min^{-1}, Q/Q$_{Max}$=1

Increasing the grid distance to the rotor, however, leads to a continuous reduction of the turbulence intensity and thus also to a reduction of the primary noise source strength for the rotors' leading edges. Incorporating the average values of the previously reported hot wire measurements, the trend of the turbulence intensity right at the rotor leading edge (Figure 6, dashed line) as a function of the grid location can be determined analytically and is shown in Figure 6. As Table 1 indicates, the grid distance is varied between 0.1 m ≤ Δz ≤ 0.5 m as it is depicted in form of the straight line in Figure 6.
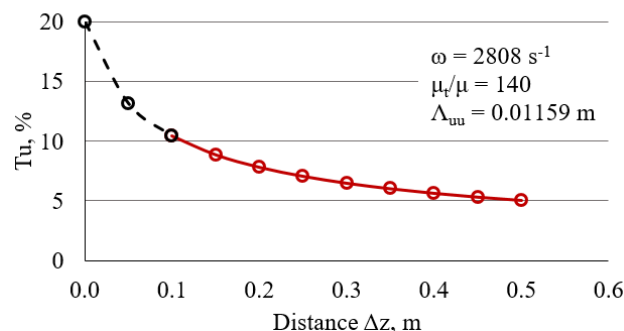

Figure 6: Analytically obtained trend of the mean turbulence intensity as a function of the distance (solid line represents used grid distance to the rotor in the current experimental setup) at given eddy viscosity ratio μ$_t$/μ, longitudinal integral length scale Λ$_{uu}$ and specific dissipation rate ω according to the power law decay model.

5 RESULTS

5.1 Effect of parameters

Based on the trained Artificial Neural Networks various contour plots, describing the influence of the analysed parameters on the response variables, can be generated. Figure 7 shows key-aerodynamic plots whereas Figure 8 shows trends on how single parameters affect the aeroacoustic response variables. The pressure rise of the fan clearly exhibits a dependency on both, fan speed and throttling state where maximum pressures are reached at maximum speed and throttling. In terms of the flow rate the dominant parameter is the throttling state, only fractionally influenced by the fan speed. In contrast to the previously described trends of approximately quadratic nature, the systems' efficiency of the analysed fan is way more complex with a maximum at high speeds but low to intermediate throttling states and a minimum at minimum speeds though high throttling states (Figure 7 – right). The grid location, however, was not found to affect the pressure rise, the flow rate or the efficiency to high degrees.

Yet, moving the focus towards aeroacoustics (Figure 8) the location of the turbulence grid does play an important role, especially at low throttling states or high flow rates, respectively. Small distances between grid and rotor lead to eddies of high energy (see also Figure 6) impinging on the rotor leading edges, causing broadband leading edge noise where larger distances lead to decreasing turbulence intensities due to dissipation according to the energy cascade and thus potential noise sources of lower energy. This pattern can be confirmed by the contour plots for both, suction noise (Figure 8 –left) and discharge noise (Figure 8 – right) even though a local maximum occurs at maximum distances for the suction side, which might be caused by model uncertainties. At high throttling states, however, no (Figure 8 - left) or only little (Figure 8 - centre) influence of the grid is visible. This is considered meaningful as at high throttling states only low axial velocities are present, leading to a sharp decrease of the turbulence generated at the grid. During the measurement campaign a clear tonal effect occurred at a fan speed of n = 1500 min^{-1} which matches the duct length resonance and accordingly leads to a maximum in terms of acceleration at the fan hub-support, independent of the throttling state, as the contour plot of the acceleration signal shows (Figure 8 - right).
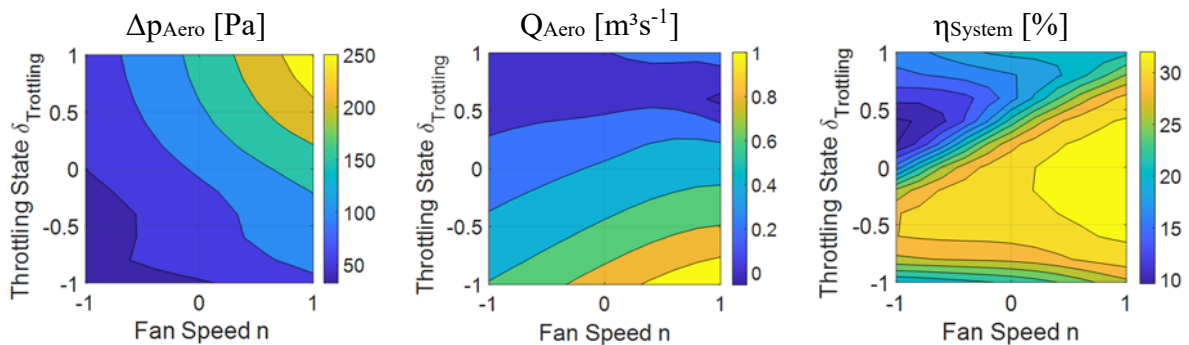

Figure 7: Contour plots of aerodynamic response variables by varying normalised parameters.
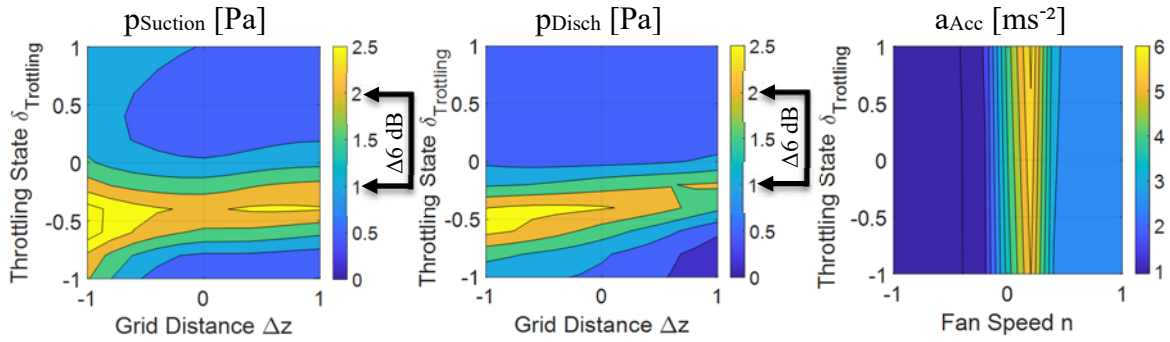
Figure 8: Contour plots of aeroacoustic/ vibroacoustic response variables by varying normalised parameters.

5.2 Comparison of Models

Three experimental designs were adopted and applied to a given system with the aim to describe it with highest possible accuracy while varying three parameters of interest. The Box Behnken Design and the Central Composite Design are used to define a model of second order while Latin Hypercube Sampling was used for the training of an Artificial Neural Network. All generated models are rated by the total fit of the model and by analysing the performance after incorporating additional independent test data. Figure 9 shows the observation/ prediction-plots for the most challenging response variables, namely the system efficiency as well as the acoustic noise radiation on the suction and on the discharge side of the fan. A perfect fit of the model is achieved when the model as well as the test data lines up along the diagonal line with small variance at a coefficient of determination $R^2 = 1$.

It can be seen that the fit of the model itself shows high values for all chosen approaches, albeit the Box-Behnken Design shows the highest values for the system efficiency and the Latin Hypercube Design fits best for the acoustic response variables. Analysing the fit of the test data, however, shows a dramatic decrease of the performance for the quadratic models but high performance for the Artificial Neural Network even though there is still space to further improve it. The performance for all response variables and approaches is summarised in Table 3. As it is already indicated by the contour plots in Figure 7 – 8, the aerodynamic trends of Δp and Q are properly describable by a quadratic model, what matches the fluid mechanics theory. On the contrary, the mapping of the system efficiency tends to be more challenging and even collapsing when it comes to aeroacoustics, requiring a more complex modelling approach. Even though the experimental effort of the LHS increases by 17% (24 → 28) for the C-CCD or 87% for the BBD (15 → 28), respectively, the performance in form of the coefficient of determination R^2 with regards to the test data for $p_{Suction}$ increases by 65% (79% $p_{Discharge}$) compared to the C-CCD approach and 59% (75% $p_{Discharge}$) compared to the BBD approach.
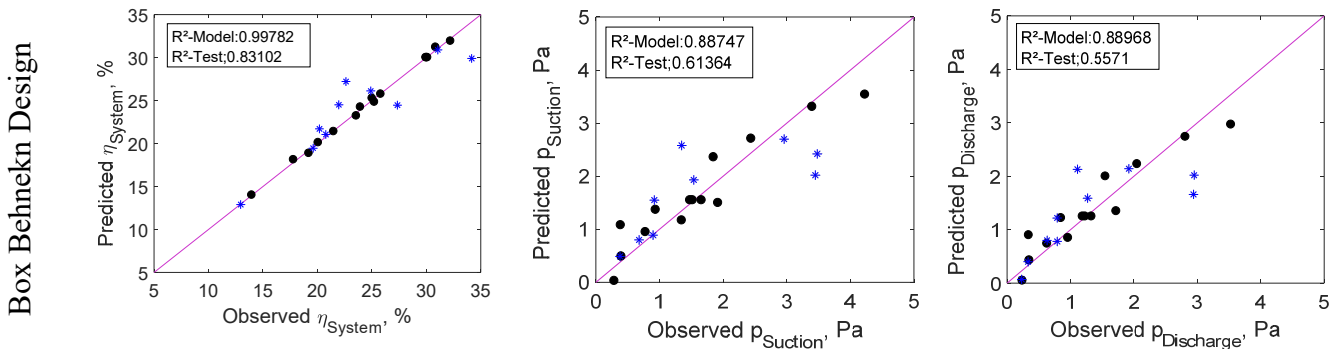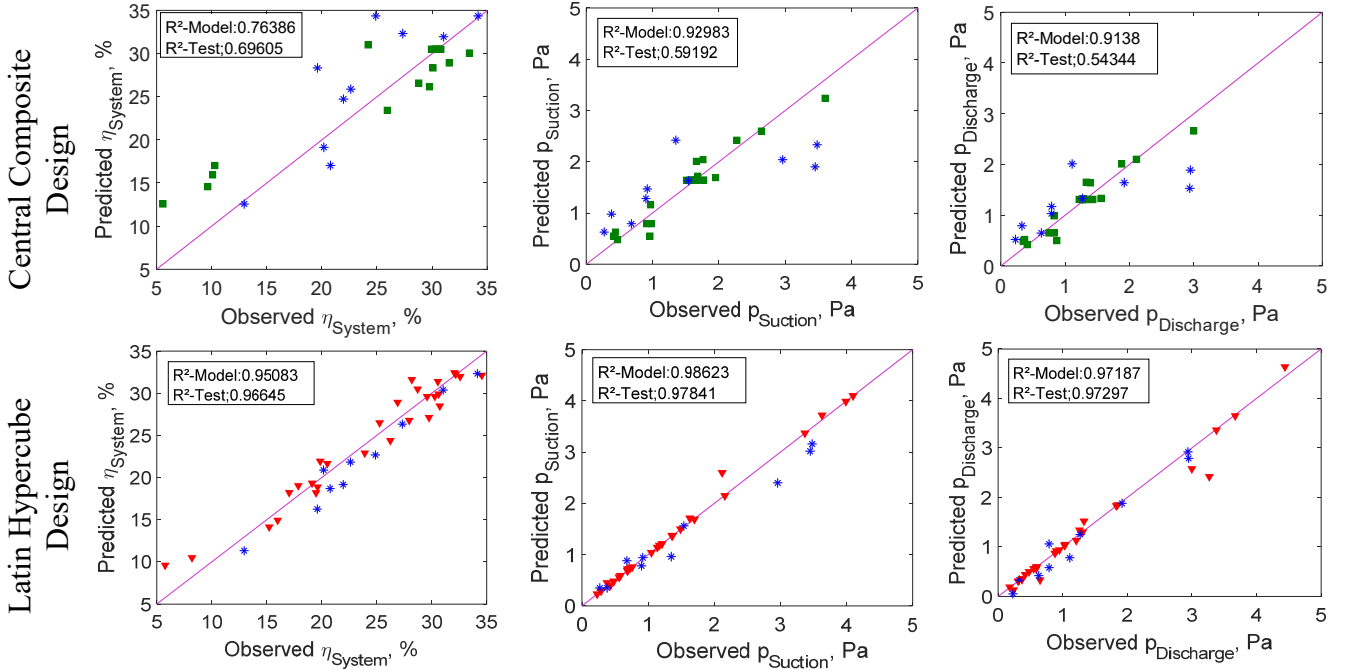
Figure 9: Observation/ Prediction-Plots, indicating the fit of the employed models. Blue stars indicate model-independent test data.

Table 3: Coefficients of performance R^2 for model data and independent test data comparing different approaches.

		No. of Samples	Δp_{Aero} [Pa]	Q_{Aero} [m³s⁻¹]	η_{System} [%]	$p_{Suction}$ [Pa]	$p_{Discharge}$ [Pa]	p_{ST} [Pa]	a_{Hub} [ms⁻²]
BBD	Model Data	15	0.999	0.995	0.998	0.887	0.889	0.879	1.000
	Test Data	10	0.993	0.991	0.831	0.614	0.555	0.555	0.648
CCD	Model Data	24	0.973	0.957	0.727	0.934	0.918	0.930	0.614
	Test Data	10	0.969	0.937	0.696	0.593	0.543	0.507	0.504
LHD	Model Data	28	0.997	0.997	0.951	0.986	0.972	0.967	0.974
	Test Data	10	0.995	0.994	0.966	0.978	0.973	0.975	0.947

5.3 Multi-Objective optimisation

It is often the case that two or more objectives are conflicting. This is especially true for aeroacoustics where the dilemma of opposing trends in terms of aerodynamics and aeroacoustics is a common challenge. That means that the optimal solution for one objective can lead to a bad solution for another objective. Computational expensive unbiased multi-objective optimisation is able to compute Pareto optimal solutions, visualised by the so-called Pareto front, which separates non-efficient from unrealisable solutions. The Pareto front also helps to indicate solutions that may be of better choice than others. Using for example ANNs with good accuracy to approximate the Pareto front is a powerful and fast way of optimising the underlying system. Figure 9 shows the Pareto front for the optimum of the system efficiency η_{System} and the acoustic radiation on the suction $p_{Suction}$ and discharge $p_{Discharge}$ side, where minimum acoustic pressures are desired while keeping the efficiency on high values. It indicates that e.g. a small reduction in efficiency of $\Delta\eta_{System} = 0.1$ % ($\eta_{System} \approx 32.5\% \rightarrow \eta_{System} \approx 32.4\%$) can lead to a tremendous reduction in acoustic radiation of $\Delta OASPL \approx 9.5$ dB ($p_{Discharge} \approx 4,5$ Pa $\rightarrow p_{Discharge} \approx 1,5$ Pa) on the discharge side of the fan.
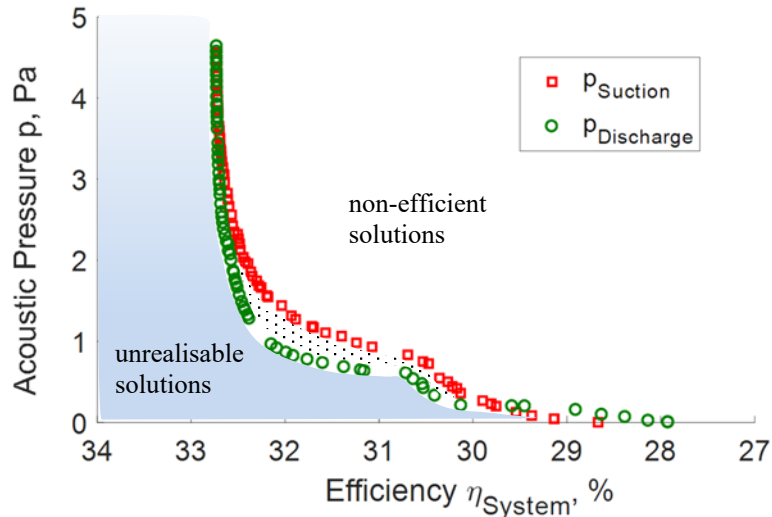
Figure 9: Pareto optimal solutions (Pareto front). Minimising the acoustic pressure while maximising the system efficiency.

6   CONCLUDING REMARKS

Detailed experiments were conducted to analyse the aerodynamic and aeroacoustic performance of an axial fan as a benchmark case. Three different approaches were analysed in terms of required experimental effort and modelling accuracy. The C-CCD and the BBD approaches are limited to models of second order whereas for the LHS in combination with an Artificial Neural Network no such restriction in model complexity is predetermined. The results obtained allow the current paper to reach the following findings:

- Latin Hypercube sampling in combination with Artificial Neural Network yields, based on the test data, an improved average performance of 44% compared to the Central Composite Design and 32% compared to the Box-Behnken Design.
- The number of model samples needed for the LHD increased by 17% (C-CCD) and 87% (BBD), respectively.
- LHD shows remarkable fit to test data, even though the levels of the test data are partly located at extreme parameter settings and are naturally hard to approximate.
- Contour plots show reasonable trends of response variables as a function of influencing parameters
- Unbiased multi-objective optimisation uncovers possibilities to achieve high efficiencies by keeping the noise radiation on low levels
- Suffering a reduction in efficiency of $\Delta\eta_{System} = 0.1\%$ leads to a reduction of the overall sound pressure level by $\Delta OASPL = 9.5$ dB.

Unpublished research based on numerical simulations indicates that it is more efficient to follow an iterative approach for finding the minimal required number of experiments for a given accuracy-level to train non-parametric approximation models than using a predefined experimental design. Consequently, after transferring this amendment to the world of experiments, where categorical and numerical factors play an important role, this approach will be adapted to upcoming research on the interaction of rotor and high-turbulent inflow conditions in terms of aerodynamics and aeroacoustics.

ACKNOWLEDGEMENTS

REFERENCES

[1] Zenger, F., Herold, G., and Becker, S., "Acoustic Characterization of Forward- and Backward-Skewed Axial Fans under Increased Inflow Turbulence," *22nd AIAA/CEAS Aeroacoustics Conference*.

[2] Amiet, R. K., "Noise Produced by Turbulent Flow into a Propeller or Helicopter Rotor," *AIAA Journal*; Vol. 15, No. 3, 1977, pp. 307–308. doi: 10.2514/3.63237.

[3] Majd Daroukh, Stephane Moreau, Nicolas Gourdain, Jean-François Boussuge, and and Claude Sensiau, "Influence of Distortion on Fan Tonal Noise,". doi: 10.2514/6.2016-2818.

[4] Biedermann, T. M., Chong, T. P., Kameier, F., and Paschereit, C. O., "Statistical-Empirical Modelling of Airfoil Noise Subjected toLeading Edge Serrations," *AIAA Journal*; Volume 55, issue 9, 2017, pp. 3128–3142. doi: 10.2514/1.J055633.

[5] Biedermann, T., Kameier, F., and Paschereit, O., "Optimised Test Rig for Measurement of Aerodynamic and Aeroacoustic Performance of Leading Edge Serrations in Low-Speed Fan Application," *Proceedings of ASME Turbo Expo 2018*, 2018.

[6] Siebertz, K., van Bebber, D., and Hochkirchen, T., *Statistische Versuchsplanung*, Springer Berlin Heidelberg, Berlin, Heidelberg, 2010.

[7] Adam, M., *Statistische Versuchsplanung und Auswertung (DoE Design of Experiments)*, University of Applied Sciences Dusseldorf, Germany, 2012.

[8] Reich, M., Adam, M., and Lambach, S., "Comparison of different Methods for Approximating Models of Energy Supply Systems and Polyoptimising the Systems-Structure and Components-Dimension," *ECOS 2017 - The 30th International Conference on Efficiency, Cost, Optimization and Environmental Impact of Energy Systems*, 2017.

[9] Alam, F. M., McNaught, K. R., and Ringrose, T. J., "A comparison of experimental designs in the development of a neural network simulation metamodel," *Simulation Modelling Practice and Theory*; Vol. 12, 7-8, 2004, pp. 559–578. doi: 10.1016/j.simpat.2003.10.006.

[10] ISO, "Acoustics – Determination of sound power radiated into a duct by fans and other air-moving devices – In-duct method (ISO 5136:2003)," 2009, No. 5136.

[11] Carolus, T. H., and Starzmann, R., "An Aerodynamic Design Methodology for Low Pressure Axial Fans With Integrated Airfoil Polar Prediction," *Volume 4: Cycle Innovations; Fans and Blowers; Industrial and Cogeneration; Manufacturing Materials and Metallurgy; Marine; Oil and Gas Applications,* ASME, 2011, pp. 335–342.

[12] Laws, E. M., and Livesey, J. L., "Flow Through Screens," *Annual Review of Fluid Mechanics*; Vol. 10, No. 1, 1978, pp. 247–266. doi: 10.1146/annurev.fl.10.010178.001335.